Heliyon 9 (2023) e17673

Contents lists available at ScienceDirect

Heliyon

journal homepage: www.cell.com/heliyon

Mathematical analysis of radius and length of CNTs on flow of nanofluid over surface with variable viscosity and joule heating

Khadija Rafique [a], Zafar Mahmood [a], Umar Khan [a,*], Sayed M. Eldin [b], Alia M. Alzubaidi [c]

[a] Department of Mathematics and Statistics, Hazara University, Mansehra, Pakistan
[b] Center of Research, Faculty of Engineering, Future University in Egypt, New Cairo, 11835, Egypt
[c] Department of Mathematics, AL-Qunfudhah University College, Umm Al-Qura University, Saudi Arabia

ARTICLE INFO

Keywords:
Nanofluids
Stretching surface
Carbon nanotubes
Variable viscosity
Joule heating

ABSTRACT

The transfer of heat is a phenomenon that is significant in a variety of contexts due to the different ways in which it may be utilized in industrial settings. To increase the rate at which heat is transferred, carbon nanotubes (CNTs), which can either be single-wall or multi-walled, are suspended in base fluids, and the resulting mixture is referred to as a "nanofluid. This study looks at how heat transfers through nanofluids that are suspended in carbon nanotubes with different lengths and radii over a stretching surface. It also looks at how changing viscosity and joule heating affect motion. Water is taken as base fluid. This study looks at both carbon nanotubes with one wall and those with more than one. The flow is governed by a series of partial differential equations, which, to control the flow, are transformed into a series of nonlinear ordinary differential equations. Similarity transformation is used to convert the obtained nonlinear ordinary differential equations and accompanying boundary conditions into a form that is dimensionless. To numerically solve the transformed equation, RK-4 with shooting method is used. Graphs and in-depth discussions are used to look at how velocity and temperature profiles are affected by the leading variables. The expression for skin friction and local Nusselt number are written down and graphs show how these two numbers change for different parameter values. The temperature profile goes down when the viscosity parameter goes down, but the velocity profile goes up. When the magnetic parameter goes up, the velocity profile $f'(\eta)$, goes down, but the velocity profile $\boldsymbol{g}(\boldsymbol{\eta})$ and temperature $\theta(\eta)$ both go up at the same time. The rate of heat transfer increases with the addition of φ and S. When the suction parameter ($S = 2.1$) with 1% of φ is used, it is reported that rate of heat transfer increases by 1.135% for Single walled and 1.275% for Multi Walled carbon nanotubes. To determine whether or not the proposed numerical model is legitimate, a comparison is made between the current results and those that have previously been published.

1. Introduction

Scientists started work on a new field of research called "nanofluids" on seeing recent progress in industries that used heat transfer.

* Corresponding author.
E-mail address: umar_jadoon4@yahoo.com (U. Khan).

https://doi.org/10.1016/j.heliyon.2023.e17673
Received 27 February 2023; Received in revised form 23 June 2023; Accepted 25 June 2023
Available online 26 June 2023

Nomenclature

a, b	constants (s^{-1})
B	magnitude of magnetic field strength
C_{fx}	Coefficient of skin friction in $x-$ ddirection (non-dimensional)
C_{fy}	Coefficient of skin friction in $y-$ ddirection (non-dimensional)
C_p	Specific heat capacitance at constant temperature $(Jkg^{-1}K^{-1})$
u_e	Free stream velocity (ms^{-1})
(ρC_p)	Fluid's heat capacitance $(JK^{-1}m^{-3})$
η	Similarity variables
k	Thermal conductivity $(Wm^{-1}K^{-1})$
M	Magnetic parameter
Nu_x	Nusselt number (non-dimensional)
Pr	Prandtl number
q_w	Surface heat flux
θ	Dimensionless temperature
μ	Dynamic viscosity $(kgm^{-1}s^{-1})$
Ec	Eckert number
Re_x	Local Reynold number in $x-$ direction (non-dimensional)
Re_y	Local Reynold number in $y-$ direction (non-dimensional)
x, y, z	Cartesian coordinates
S	Mass transportation parameter (non-dimensional)
t	Time (s)
T	Temperature (K)
T_0	Reference temperature of sheet (K)
T_w	Temperature at stretching/shrinking surface (K)
T_∞	Ambient temperature (K)
u, v, w	velocity component in the x $-$, $y-$ and z $-$ directions (ms^{-1})
w_w	Mass suction velocity (ms^{-1})
v_w	Surface velocity of the stretching/shrinking surface (ms^{-1})
θ_r	Viscosity parameter
ν	Kinematic viscosity (m^2s^{-1})
ρ	Density (kgm^{-3})
φ	Nanoparticle volume fraction of CNTs (%)
τ	Dimensionless time variable $(-)$
τ_w	Wall shear stress (Nm^{-2})
λ	Stretching/shrinking parameter $(-)$
f	Base fluid
nf	nanofluid

Choi and Eastman [1] came up with the term "nanofluids" to describe fluids with particles that measures just few nano size particles. Fluids like water, kerosene oil, and engine oil don't carry heat or electricity very well. Choi et al. [2] suggested some changes to improve their thermal properties and make up for their low thermal conductivity. Nanofluids are now commonly used in industry. They can be used to make glasses that can't be scratched, to kill bacteria, and to coat plastic and fabrics to protect them from ultraviolet light. After Choi's groundbreaking work, many other researchers made different models that also considered the shape, size, type, and other properties of nanoparticles. Buongiorno [3] made a model that is more complete and take into account Brownian motion and thermophoresis. When Hamilton and Crosser [4] added the size, type and shape of nanoparticles to their model they showed us a new way to think about nanofluids. In Ref. [5] researcher found discharge of energy storage unit with addition of nanoparticles. Li et al. [6] looked at nanomaterial inclusion for thermal storage system. Othman et al. [7] used numerical simulation for nanomaterial efficacy. Li et al. [8] numerically studied the nanoparticles dispersion in solidi cation. Buongiorno's model to figure out how a nanofluid flows at the edge of a stretched sheet. Researchers have looked at the energy storage system with inclusion of nanomaterial and existence of nanosized additives by mean of numerical method in Refs. [9,10].

In recent studies, carbon nanotubes have been looked at as nanoparticles because they conduct heat better than other fluids. CNTs are tubes made from graphene sheets that are rolled into tubes. Iigima made the first ones in 1991. Carbon nanotubes can be either single-walled or many-walled. Nanotubes can be longer than 1 μm and have a diameter of 1 nm, which is smaller than the diameter of high-tech semiconductor devices. The way carbon nanotubes carry electricity is also different from how other semiconductors do it. Popov [11] and Taherian et al. [12] did research on carbon nanotubes' special properties and reviews. Researchers did a lot of work to figure out how the presence of carbon nanotubes and other things in fluid affect how fluids flow. The RBF approach was used by Falah

et al. [13] to investigate how nanofluid flows in channels. The Christof heat flux of stretching sheets with suspended CNT and MHD flow was examined by Shakuntala et al. [14,15]. Akbar et al. [16] used a homogeneous model to look at the flow of carbon nanotubes at the stagnation point toward a stretching sheet. Researchers found that stronger magnetic field slows down rate of heat transfer at surface and single-walled carbon nanotube transfer heat faster than carbon nanotube with more than one wall. Later, Hayat et al. [17] looked at the flow at stagnation point on stretching surface with both homogeneous and heterogeneous reaction. They used a similar CNTs nanofluid to do this. Nanddeppavar et al. [18] investigated the movement of carbon nanotube-suspended nanofluids while they were subjected to the effects of velocity slip. In a porous medium, Sreedevi et al. [19] looked at how nanofluids with CNTs move heat and mass towards vertical cone. They did this by looking at magnetic field, the chemical reaction and the parameters for suction and injection. The results showed that rate of heat transfer is better when volume fraction of nanoparticles is higher, and that rate of heat transfer is better when multi-walled CNT are used as nanoparticles instead of single-walled CNT. Researchers Shaku Thala et al. [20], studied heat transfer and Blasius flow as a result of a moving plate.

There has been a lot of research on heat transfer and flow of surface that stretches and contracts because of its industrial uses, such as in electrical applications, getting polyethylene strips, making decorations, and making paper and pulp. Nanddeppavar [21] investigated the melting heat transfer in Casson fluid induced by a moving plate. This was one of the things that he investigated. In addition to this, they investigated double diffusive free convection caused by a sliding vertical plate in the presence of nonlinear thermal radiation [22]. The effects of velocity slip and thermal slip on nanofluid as it moves past a stretched cylinder were investigated by Ashish Mishra and Manoj Kumar [23]. In Refs. [24,25], the researchers looked into the influence that thermal radiation and viscous dissipation had on the flow of nanofluid across a stretched sheet and on a Riga plate. Similar findings have been discovered by past studies when it comes to shrinking sheets. In the literature, there are several outstanding evaluations of flow caused by a stretching/shrinking surface. Faghiri et al. [26] investigated the flow of non-Newtonian fluid through a circular tube while the tube was subjected to wall heat flux. Akbari et al. [27] investigated non-Fourier heat conduction in hollow spheres with temporally and spatially variable boundary conditions. The flow of a second-grade viscoelastic nanofluid was investigated by Hossein Zadeh and colleagues [28] on a curved and stretched surface. After that, Ashish Mishra and Kumar [29] investigated the impact of viscous dissipation and heat generation on nanofluid flow across a wedge using numerical simulations.

Eringen [30] found that fluid's physical properties change a lot as temperature goes up or down. When the temperature goes up, there are more transport phenomena because the viscosity of momentum boundary layer goes down. This affects rate of heat transfer at wall. The viscosity of the fluid needs to be taken into account if flow and heat transfer rates are to be accurately predicted. The reason for this is that viscosity changes with temperature. Salem [31] investigated how MHD flow and heat transfer in a viscoelastic fluid across a stretching sheet are affected by the viscosity of the fluid as well as the thermal conductivity of the fluid. In metallurgy and chemical engineering, it is useful to know how properties change with temperature. For example, in the extrusion process, materials that have been heated and are moving on a conveyor belt between wind-up roll and a feed roll have a smooth, moving surface. Temperature affects rate of heat transfer at wall by speeding up local transport phenomena and making the momentum boundary layer less viscous. The viscosity variation must be considered when predicting the flow behaviour of fluids that could not be compressed [32]. Analytical analysis was used by Attar et al. [33] to investigate the solution of a fractional differential equation. Mehta and Sood [34] presented that when this effect is considered, flow characteristics can be very different from what they were when the viscosity was thought to be constant. Lubricating fluids can no longer be assumed to have the same viscosity because heat from internal friction and the resulting rise in temperature change the viscosity. Alipour et al. [35] investigated the behavior of a mixture of hybrid nanofluids by optimizing their behavior in a porous cavity. Mukhopadhyay and Layek [36] and others looked at the effects of temperature-dependent viscosity and thermal conductivity on flow and heat transfer over a stretching surface for different fluids and flow situations. The rise in temperature is what causes the change in viscosity across the moment-to-moment boundary layer.

By running an electric current through a resistor, you can use the Joule effect to make heat. "Ohmic heating" is another name for this. Many things, like incandescet light bulbs, ovens, electric heaters and electric stove use joule heating [37]. In their study, Talebi Rostami and colleagues [38] investigated the flow of a mixture-based, dusty hybrid nanofluid that was induced by a magnetic field. Yan et al. [39], looked at a steady MHD hybrid nanofluid flow that moves through surface and is heated by Joule. Observations of the first solution showed that magnetic and suction parameter made skin friction coefficient go up, but the velocity slip factor made it go down. Dual solution temperature goes up as Eckert number goes up. But the distance between the boundary layers didn't change when the Eckert number parameters were changed. Gulzar et al. [40] investigated the effects of thermal stratification and a magnetic field on the movement of heat within a magnetohyperbolic tangent liquid. Researchers Cao et al. [41] investigated how the presence of a magnetic field affected the behavior of laminar flow and convective heat transfer. Yan et al. [39], came to conclusions about how the Eckert number affect temperature of dual solution. Also, Eckret number had no effect on the change in reduced skin friction, which stays the same as the Eckert number goes up. Adnan et al. [42], looked at flow of three-dimenssional hybrid nanofluid with a rotating sheet that stretches and contracts while a magnetic field and joule heating are present.

On the other hand, a closer analysis of the works that have been published on the themes exposes various gaps and contradictions in the information that they present. These problems may be seen in the material that is presented in these works. In the prior references, heat transfer through nanofluids that are suspended in carbon nanotubes was the main topic of discussion; however, gaps can be filled to meet the condition for further investigation. In practical, heat transfer is not limited to nanofluid in carbon nanotubes with same length and radius. So far as we know, no previous research has looked at the heat transfer through nanofluids that are suspended in carbon nanotubes over a stretching surface with different length and radii having joule heating and changing viscosity. In light of the previous research, the aim of this work is to investigate the influence of joule heating and changing viscosity on the flow of carbon nanotube suspended nanofluid with varying length and radius over a surface that is stretched. The resulting nonlinear ordinary differential equations and associated boundary conditions are transformed into the dimensionless form using similarity transformation.

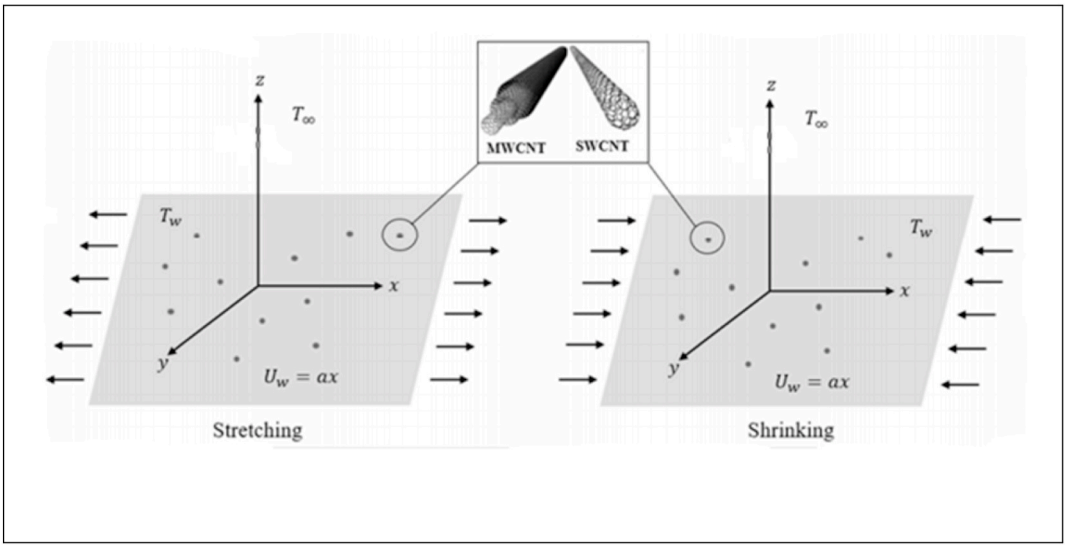

Fig. 1. Physical model diagram.

Transformed equation are then solved numerically by RK-4 with shooting method. Graphs show effects of different controlling parameters on dimensionless velocity, temperature, and skin friction cofficients. Lastly, a graph shows how different parameters affect local skin friction cofficients and local Nusselt number. The analysis shows that fluid flow is appreciably influenced by physical parameters. When the viscosity parameter goes down, the velocity profile goes up while temperature profile go down. The volume percentage of nanoparticles causes the velocity profiles to drop while simultaneously increasing the temperature profile. There is a chance that this contribution will help boost industrial output, most notably in the manufacturing and process industries. Finding out how nanofluids move while they are suspended in carbon nanotubes of varying lengths and radii is the objective of this research. If the findings are successful, the nanofluids may find applications in both medical and industrial contexts. The findings of this research might be put to use in the development of a thermal process that is efficient and makes effective use of the most effective physical sources, such as heat pumps and refrigerants. The plan is as follows:

- ➢ Nanofluids should be stimulated while they are suspended in carbon nanotubes of varying lengths and radii.
- ➢ Find out how joule heating affects the heat transfer.
- ➢ Find out how changing viscosity affects the flow.

2. Description of the problem

Fig. 1 depicts the three-dimensional MHD CNTs (SWCNT & MWCNT) suspended nanofluid flow with different length and radius over a stretching sheet that can be shown in three dimensional cartesian coordinate system. At $z \geq 0$ it is thought that the CNTs (SWCNT and MWCNT) in the nanofluid are moving in a laminar, Newtonian, steady, and incompressible flow. Both $x-$ axis and $y-$ axis is measured in plane where $z = 0$. Following assumptions are made for sheet at $= 0$.

I. It is assumed that sheet is stretched/shrinked in $x -$ direction with velocity $u_w = ax$ where a is constant.
II. Magnetic field having strength B that is applied along the $z-$ axis influences it.

$T_w = T_0 x^2$, gives the temperature of a sheet that is growing or shrinking where T_0 is the characteristic temperature and ambient temperature is denoted by T_∞. To reach a state of thermal equilibrium, you need both nanoparticles and fluid phases. Also, velocity slip between the phases doesn't need to be considered because all the nanoparticles are the same shape and size.

Th basic equations for conservation of mass, momentum and thermal energy can be used to describe the above model (see Ref. [42]).

$$\frac{\partial u}{\partial \mathrm{x}} + \frac{\partial v}{\partial \mathrm{y}} + \frac{\partial w}{\partial z} = 0, \tag{1}$$

$$u\frac{\partial u}{\partial \mathrm{x}} + v\frac{\partial u}{\partial \mathrm{y}} + w\frac{\partial u}{\partial z} = \frac{1}{\rho_{cnt}}\frac{\partial}{\partial z}\left(\mu_{cnt}\frac{\partial u}{\partial z^2}\right) - \frac{\sigma_f}{\rho_f}B_0^2 u, \tag{2}$$

Table 1
Table of thermophysical properties of different CNTs with base fluid (see Ref. [43]).

Properties	*SWCNT*	*MWCNT*	Water
$\rho\,(kg/m3)$	2600	1600	997.1
$Cp\,(J/kgK)$	425	796	4179
$k\,(W/mK)$	6600	3000	0.613
Pr			6.2

Table 2
The effective thermophysical properties of CNTs suspended Nanofluid (see Refs. [43,44]).

Density	$\rho_{cnt} = (1-\varphi)\rho_f + \varphi\rho_s,$
Viscosity	$\mu_{cnt} = \frac{\mu_f}{(1-\varphi)^{2.5}},$
Heat capacity	$(\rho C_p)_{cnt} = (1-\varphi)(\rho C_p)_f + \varphi(\rho C_p)_s,$
Thermal Conductivity (Yamada-Ota Model)	$\frac{k_{cnt}}{k_f} = \frac{1+\frac{k_f}{k_s}\frac{L}{R}\varphi^{0.2} + \left(1-\frac{k_f}{k_s}\right)\varphi\frac{L}{R}\varphi^{0.2} + 2\varphi\left(\frac{k_s}{k_s-k_f}\right)ln\left(\frac{k_s+k_f}{2k_s}\right)}{1-\varphi+2\varphi\left(\frac{k_f}{k_s-k_f}\right)ln\left(\frac{k_s+k_f}{2k_s}\right)}.$

$$u\frac{\partial v}{\partial x}+v\frac{\partial v}{\partial y}+w\frac{\partial v}{\partial z}=\frac{1}{\rho_{cnt}}\frac{\partial}{\partial z}\left(\mu_{cnt}\frac{\partial v}{\partial z^2}\right)-\frac{\sigma_f}{\rho_f}B_0^2 v, \tag{3}$$

$$u\frac{\partial T}{\partial x}+v\frac{\partial T}{\partial y}+w\frac{\partial T}{\partial z}=\frac{k_{cnt}}{(\rho C_p)_{cnt}}\frac{\partial^2 T}{\partial z^2}+\frac{\sigma_f}{\rho_f}B^2\left(u^2+v^2\right). \tag{4}$$

u, v and w denotes velocity component along three axes: respectively x, y and z.
Next, the boundary conditions are (see Ref. [42]):

$$\left.\begin{array}{c} u=\lambda u_w, v=by, w=w_w, T=T_w \;\; at\; z=0, \\ u\to 0, v\to 0, T\to T_\infty \;\; as\; z\to\infty. \end{array}\right] \tag{5}$$

Nanofluid temperature is T, μ_{cnt} is dynamic viscosity, ρ_{nf} is density, thermal conductivity is k_{cnt} and heat capacity $(\rho C_p)_{cnt}$. In addition, λ is the constant parameter for stretching and shrinking with the value of $\lambda = 0$ indicating static sheet, $\lambda < 0$ for shrinking case, and $\lambda > 0$ indicating stretching.

Table 1 gives different thermophysical properties of single wall, multi-walled carbon nanotubes, base fluid(water). In Table 1 ρ, is density, Cp, is heat capacity, k, is thermal conductivity and Pr is Prandtl number for base fluid. Table 2 shows thermophysical properties of nanoparticles suspended based nanofluids. In Table 2 ρ_{cnt}, shows density of carbon nanotubes, μ_{cnt}, shows viscosity of carbon nanotubes, $(\rho C_p)_{cnt}$, is heat capacity and $\frac{k_{nf}}{k_f}$, is ratio of thermal conductivity of nanofluid to base fluid. In this work, thermal property of CNTs was analyzed by using Yamada- Ota thermal conductivity model. Inserting a thermal conductivity correlation into the energy equation that is dependent on length and radius of carbon nanotubes helps to increase the thermal conductance of the material. The nanofluid model that was described before is both highly linked and tedious. Due to the characteristics of the nanofluid model, analytical solutions cannot be relied upon. As a result, the numerical approach is the most effective method for dealing with such a nanofluid model. The flow model was simplified into a form that was comparable to itself using transformations that were practical, and it was then treated numerically.

When calculating these equations, several variables must be considered. φ, is solid volume part of nanofluid, effective nanofluid has a dynamic viscosity μ_{nf} and μ_f is the viscosity coefficient which is consider varying in inverse relation with temperature as follows (see Ref. [45]):

$$\frac{1}{\mu_f}=\frac{1}{\mu_{f_\infty}}[1+\delta(T-T_\infty)] \text{ i.e.,} \frac{1}{\mu_f}=\alpha(T-T_r), \tag{6}$$

here

$$\alpha=\frac{\delta}{\mu_{f_\infty}}, T_r = T_\infty - \frac{1}{\delta}$$

In most applications, reference temperatures chosen for correlations are very practical. Here α and T_r are constants, and it depends on thermal property of fluid and reference position i.e., δ (a constant) overall, for liquid > 0 and $\alpha < 0$ for gases. T is temperature, T_∞ and μ_{f_∞} are constant values of viscosity coefficient and temperature respectively, distant from the surface. Density of base fluid is ρ_f. ρ_{nf} nanofluid density, $((\rho C_p)_{nf})$ is heat capacity of nanofluids. k_{nf} is thermal conductivity of nanofluids and in basic fluids it is represented by k_f.

Introducing the dimensionless velocities, temperature, and variable η as (see Ref. [42]):

$$u = axf'(\eta), v = byg(\eta), w = -\sqrt{av}(f(\eta)), \theta(\eta) = \frac{T - T_\infty}{T_w - T_\infty}, \eta = \sqrt{\frac{a}{\nu_f}}z. \tag{7}$$

and $w_w = -\sqrt{av_f}S$ mass flux velocity constant, where $S = f(0)$ in which $S > 0$ shows suction and $S < 0$ shows injection.

Where prime shows differentiation in relation to η. In perspective of Eq. (7), Eqs. (1)–(5) are reduced to the following boundary value problem:

$$\frac{f'''}{1-\frac{\theta}{\theta_r}} + \frac{f''\theta'}{\theta_r\left(1-\frac{\theta}{\theta_r}\right)^2} = -A_1A_2\left[(f)f'' - f'^2 - Mf',\right. \tag{8}$$

$$\frac{g''}{1-\frac{\theta}{\theta_r}} + \frac{g'\theta'}{\theta_r\left(1-\frac{\theta}{\theta_r}\right)^2} = -A_1A_2\left[(f)g' - f'g - Mg,\right. \tag{9}$$

$$A_3\theta'' + Pr\,A_4\left[(f)\theta' - 2f'\theta + MEc\left(f'^2 + g'^2\right)\right] = 0, \tag{10}$$

Here

$$A_1 = (1-\varphi)^{2.5}, \text{(For SWCNT \& MWCNT Model)},$$

$$A_2 = (1-\varphi) + \varphi\frac{\rho_S}{\rho_f}, \text{(For SWCNT \& MWCNT Model)},$$

$$A_3 = \frac{1 + \frac{k_f}{k_s}\frac{L}{R}\varphi^{0.2} + \left(1-\frac{k_f}{k_s}\right)\varphi\frac{L}{R}\varphi^{0.2} + 2\varphi\left(\frac{k_s}{k_s-k_f}\right)ln\left(\frac{k_s+k_f}{2k_s}\right)}{1-\varphi + 2\varphi\left(\frac{k_f}{k_s-k_f}\right)ln\left(\frac{k_s+k_f}{2k_s}\right)} \text{ (For SWCNT \& MWCNT Model)},$$

$$A_4 = (1-\varphi) + \varphi\frac{(\rho C_p)_S}{(\rho C_p)_f} \text{ (For SWCNT \& MWCNT Model)}.$$

Boundary conditions transformation (5) into

$$f(0) = S, g(0) = 1, f'(0) = \lambda, \theta(0) = 1,$$

$$f'(\eta) \to 0, g(\eta) \to 0, \theta(\eta) \to 0, as\ \eta \to \infty. \tag{11}$$

In the previous equations, $Pr = \frac{(\rho C_p)_f}{k_f}$ shows the Prandtl number and parameter of suction/injection is indicated by S, where $S > 0$ shows suction and $S < 0$ shows injection. $\theta_r = -1/[\delta(T_w - T_\infty)]$ is parameter of fluid viscosity. $M = \frac{\sigma_f B_0^2}{\rho_f a}$ is magnetic parameter and $Ec = \frac{a^2}{T_0(C_p)_f}$ is the Eckert number.

The friction coefficients Cf_x and Cf_y along the x axes, y axes and local Nusselt number Nu_x, is the most important in the investigation (see Ref. [42]).

$$C_{fx} = \frac{\tau_{\tilde{w}x}}{\rho_f u_w{}^2}, C_{fy} = \frac{\tau_{\tilde{w}y}}{\rho_f u_w{}^2}, N\tilde{u}_x = \frac{xq_{\tilde{w}}}{k_f(T_w - T_\infty)}. \tag{12}$$

Where $\tau_{\tilde{w}x}$, $\tau_{\tilde{w}y}$ symbolize the shear stresses on x and y axes, respectively, and $q_{\tilde{w}}$ symbolize the heat flux. These terms are written below (see Ref. [42]):

$$\tau_{\tilde{w}x} = \mu_{cnt}\left(\frac{\partial u}{\partial z}\right)_{z=0}, \tau_{\tilde{w}y} = \mu_{cnt}\left(\frac{\partial v}{\partial z}\right)_{z=0}, q_{\tilde{w}} = -k_{cnt}\left[\left(\frac{\partial T}{\partial z}\right)_{z=0}\right]. \tag{13}$$

By provoking equations (7), (12) and (13) we get the following (see Ref. [42]):

$$Re_x^{1/2}C_{fx} = \frac{1}{A_1\left(1-\frac{\theta}{\theta_r}\right)}f''(0), Re_y^{1/2}C_{fy} = \frac{1}{A_1\left(1-\frac{\theta}{\theta_r}\right)}g'(0),$$

$$Re_x^{-1/2}Nu_x = -A_3\theta'(0), \tag{14}$$

Table 3
$f^{'}(0)$ and $g^{''}(0)$ when $S = M = Ec = \theta_r = \varphi =$ and $\lambda = 1$ (stretched case).

	$f^{'}(0)$	$g^{'}(0)$
Present Study (shooting)	1.1737223	1.1737223
Wahid et al. [46] (bvp4c)	1.173721	1.173721
Khashi'ie et al., [47] (bvp4c)	1.173721	1.173721

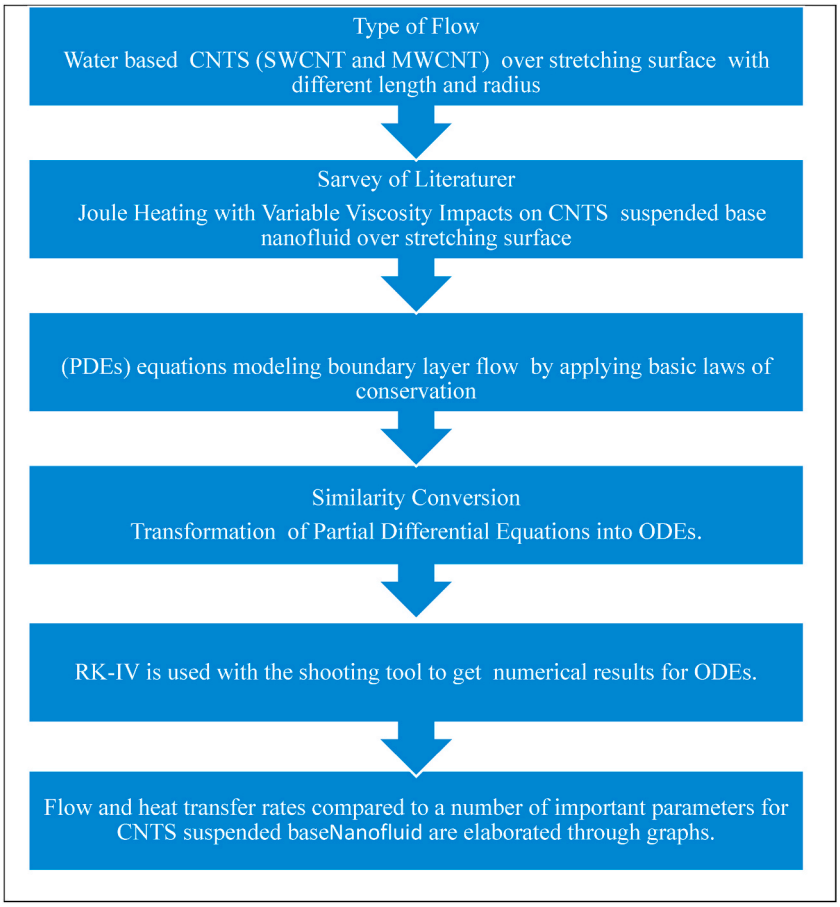

Fig. 2. Mathematical demonstration of problem.

where $Re_x = \frac{ax^2}{\upsilon_f}$ and $Re_y = \frac{by^2}{\upsilon_f}$ denotes local Reynolds numbers on the x and $y-$ axes, respectively.

3. Solution methodology and code validation

The coupled ordinary differential equations 8–10 and related boundary conditions (11) are nonlinear and very complex. It is preferable to use a numerical scheme to solve these equations. To capture the various physical variables for the flow paths of nanofluid we will use the combined RK and shooting method (see Refs. [43,48,49]). The Runge-Kutta technique can be applied to build a high-order accurate numerical approach by the functions themselves, and this can be done without the need for the high-order derivatives of the functions. Depending on order to which same momentum and energy equations 8–10 are used, several transformations are required to begin the process, as well as the boundary domains contained in equation (11). These modifications reduced complex model to initial value problem which is solved easily as follows (see Refs. [43,48,49]):

$$\Xi_1 = f, \Xi_2 = f^{'}, \Xi_3 = f^{''}, \Upsilon_1 = g, \Upsilon_2 = g^{'}, \Upsilon_3 = g^{''}, \Lambda_1 = \theta, \Lambda_2 = \theta^{'}, \tag{15}$$

using equation (15),

$$\Xi_1^{'} = f^{'}, \Xi_2^{'} = f^{''}, \Xi_3^{'} = f^{'''}, \Upsilon_1^{'} = g^{'}, \Upsilon_2^{'} = g^{''}, \Upsilon_3^{'} = g^{'''}, \Lambda_1^{'} = \theta^{'}, \Lambda_2^{'} = \theta^{''}, \tag{16}$$

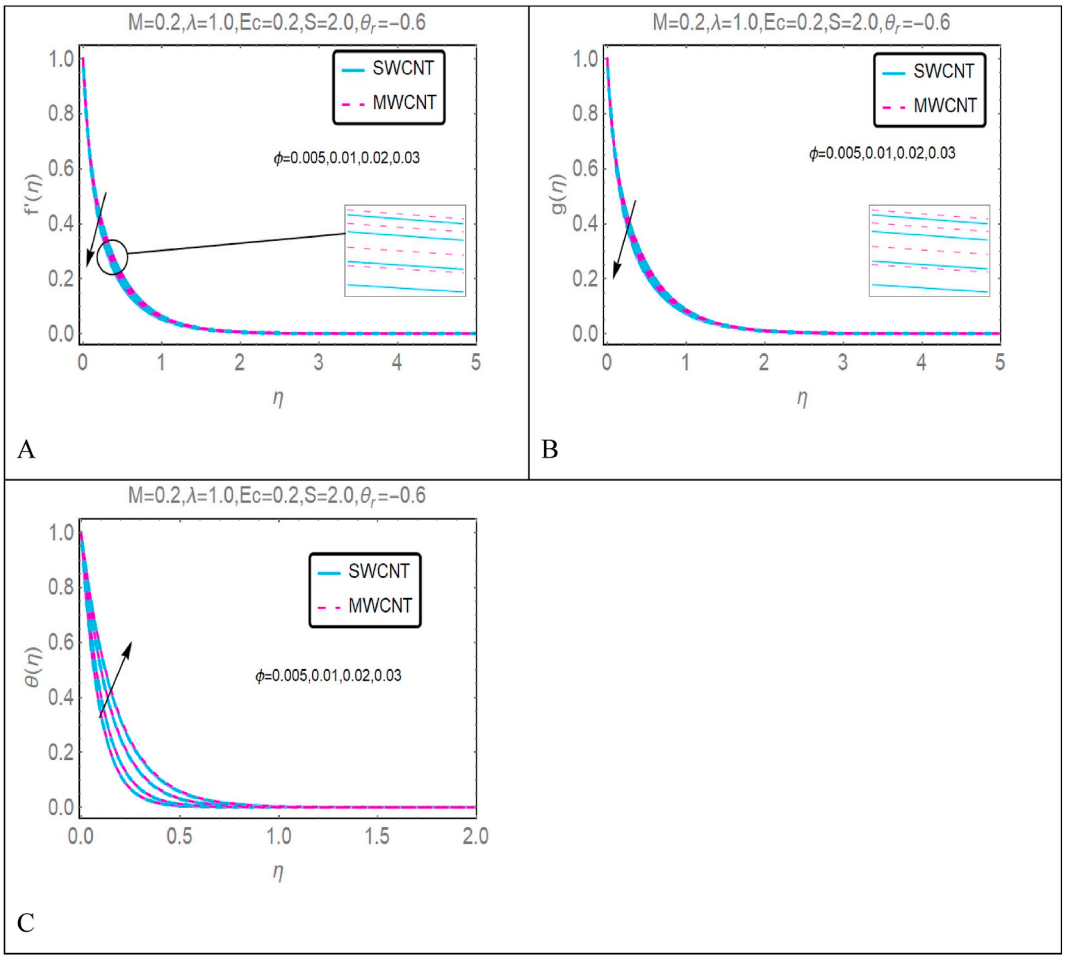

Fig. 3. **(A):** Impact of φ on $f'(\eta)$. **(B):** Impact of φ on $g(\eta)$. **(C):** Impact of φ on $\theta(\eta)$..

we are getting the following results from equations (15) and (16).

$$\Xi_1' = \Xi_2, \Xi_2' = \Xi_3, \Xi_3' = f''', \Upsilon_1' = \Upsilon_2, \Upsilon_2' = \Upsilon_3, \Upsilon_3' = g''', \Lambda_1' = \Lambda_2, \Lambda_2' = \theta'', \tag{17}$$

Due to the complexity of the model, we limited ourselves to defining the transformations and incorporating the findings for the various flow regimes. Mathematica is utilized for any further computations that need to be performed. By arranging equations 8–10 as bellow, we will obtain the values of f''', g''' and θ'' that appear in equation (17):

$$f''' = -\left(1-\frac{\theta}{\theta_r}\right)\left[\frac{f''\theta'}{\theta_r\left(1-\frac{\theta}{\theta_r}\right)^2} + A_1A_2\left[(f+g)f'' - f'^2 + 2\lambda g' - \frac{B_1}{A_2}\mathrm{M}f'\right]\right., \tag{18}$$

$$g''' = -\left(1-\frac{\theta}{\theta_r}\right)\left[\frac{g''\theta'}{\theta_r\left(1-\frac{\theta}{\theta_r}\right)^2} + A_1A_2\left[(f+g)g'' - g'^2 - 2\lambda f' - \frac{B_1}{A_2}\mathrm{M}g\right]\right., \tag{19}$$

$$\theta'' = -\frac{1}{A_3}\left[Pr\,A_4\left[(f)\theta' - 2f'\theta + MEc\left(f'^2 + g'^2\right)\right]\right] \tag{20}$$

For solving the initial value problem, we must incorporate the values from equations (15) and (17) into equations 19 and 20, respectively. Mathematica 10, a powerful computational software package, is used to obtain numerical solutions for (18–20). It has the distinct property of classifying the main system of equation and applying the most appropriate numerical method to give an accurate solution of the problem. Because most numerical methods are impractical to deal semi-infinite problems and the infinite norm is

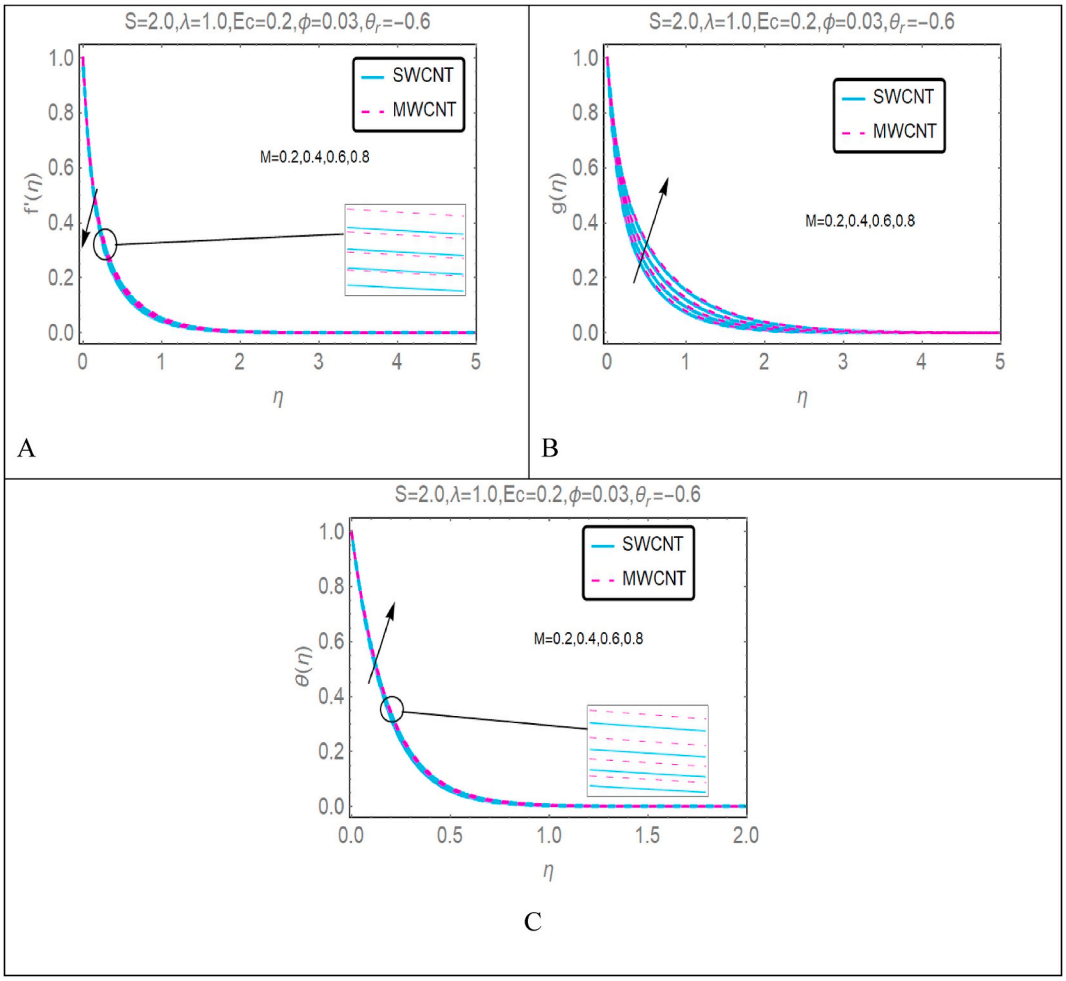

Fig. 4. **(A):** Impact of M on $f^{'}(\eta)$. **(B):** Impact of M on $g(\eta)$. **(C):** Impact of M on $\theta(\eta)$..

replace by the proper finite value of η, due to which no key change in the system of physical phenomenon are observed.

To validate the results of this study, a comparison analysis was carried out between the values of $f^{''}(0)$ and $g^{''}(0)$ that were acquired in the current investigation and the previously developed related models, which are tabulated in Table 3. The values that were compared were found to have a high degree of agreement, which served to validate the numerical answers as well as the numerical method that was used.

4. Results and discussion

Equations (8)–(11) are resolved in computer programme Mathematica using the shooting method with the RK-IV; more details are given in the preceding section. Figures and tables display the numerical results. Fig. 1 shows the physical situation of the problem and Flowchart that depicts Mathematical demonstration of problem is shown in Fig. 2. Figs. 3–10 provide a thorough view of current condition by illustrating the effects of velocity, temperature, skin friction and Nusselt number. Carbon nanotubes suspended base nanofluid are used in the analysis. The ranges of values for the control parameters are changed in accordance with what is shown in the tables and graphs. The selection of these values is determined by whether the far-field boundary criteria are satisfied (11).

4.1. Velocity $f^{'}(\eta)$, $g(\eta)$ and temperature profile $\theta(\eta)$

Figs. 3–6 depict effects of several factors, such as: volume fraction φ viscosity parameter θ_r, magnetic field M, Eckert number Ec suction S, and stretching parameter λ on velocity $f^{'}(\eta)$, $g(\eta)$ and temperature $\theta(\eta)$ for evaluation of carbon nanotubes suspended. The Prandtl number is set to 6.2 because water is used as base fluid. Both SWCN and MWCNT are used to make nanoparticles. In Table 1, both base fluid and nanoparticles' thermophysical properties are listed. In the flow analysis, solid line on graphs shows SWCNS and dashed line shows the MWCNT. Fig. 3A shows effect of nanoparticles volume fraction φ on dimensionless velocity $f^{'}(\eta)$ when it varies

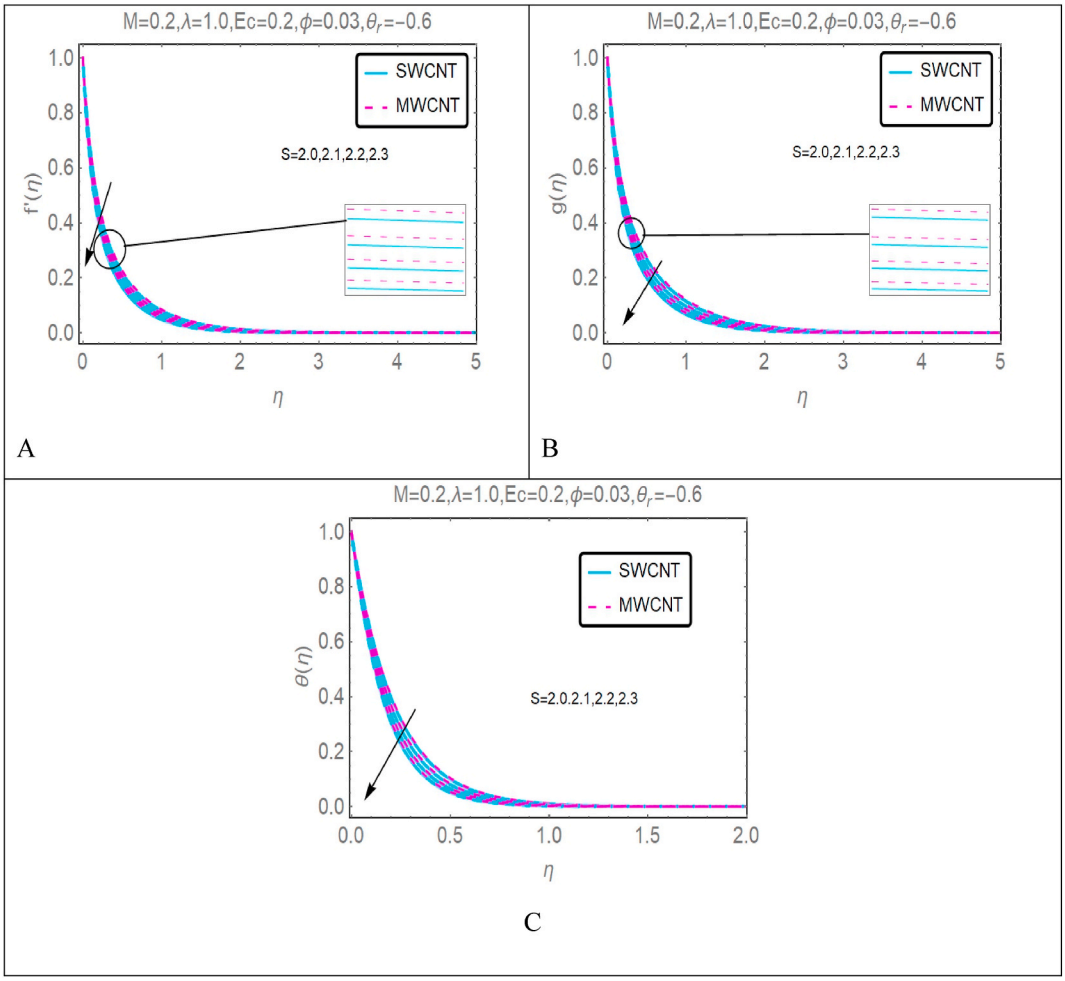

Fig. 5. **(A):** Impact of S on $f'(\eta)$. **(B):** Impact of S on $g(\eta)$. **(C):** Impact of S on $\theta(\eta)$..

from 0.005 to 0.03 respectively for stretching case when $S = 2.0, \lambda = 1.0, M = 0.2, Ec = 0.2, \theta_r = -0.6$. Fig. 3B show impact of volume fraction φ on velocity profile $\boldsymbol{g}(\boldsymbol{\eta})$ and Fig. 3C demonstrates impact of volume fraction φ on temperature profile $\theta(\eta)$. 3 A shows that when volume fraction φ increases from 0.005 to 0.03 then velocity profile $f'(\eta)$ decreases. Velocity decreases when concentration of nanoparticles increases. Fig. 3B shows that when volume fraction φ increases then velocity profile $\boldsymbol{g}(\boldsymbol{\eta})$ decreases. Fig. 3C demonstrates temperature profile $\theta(\eta)$ increases when volume fraction parameter φ increases from 0.005 to 0.03. Observations reveal that when volume fraction rises, velocity profile in carbon nanotubes suspended based nanofluid decreases while temperature profile rises, and the layer thickness become more evident. These figures make it very evident that the velocity profiles decrease, and temperature curve rises as volume percent increases. Improvements in volume fraction resulted in an increase in nanofluid viscosity, which, as response of their respective impacts on flow velocity profile, slowed the flow. Increasing the value of nanoparticles volume fraction rising temperature profile. Physically this is owing to augmentation of thermal conductivity in presence of more fragments.

Fig. 4 shows impact of magnetic parameter M on velocity profile $f'(\eta)$, $\boldsymbol{g}(\boldsymbol{\eta})$ and temperature profile $\theta(\eta)$. Fig. 4A shows impact of M, on $f'(\eta)$, when it varies from 0.2 to 0.8 and $S = 2.0, \lambda = 1.0, E_c = 0.2, \varnothing = 0.03, Ec = 0.2, \theta_r = -0.6$. Fig. 4B shows impact of varying M, on $\boldsymbol{g}(\boldsymbol{\eta})$. Fig. 4C shows the graph of M, and temperature profile $\theta(\eta)$. 4 A demonstrates that when magnetic parameter s increasing from 0.2 to 0.8 then velocity profile $f'(\eta)$ is decreasing. This is because the presence of magnetic field produces resistive force. This force act in opposite direction to motion of fluid thereby causing deceleration of $f'(\eta)$. 4B demonstrates that when magnetic parameter M increases then velocity profile $\boldsymbol{g}(\boldsymbol{\eta})$ increases. 4C shows when magnetic parameter increases from 0.2 to 0.8 then temperature profile $\theta(\eta)$ also increases. This is due to energy produced by Lorentz force in presence of magnetic field which is applied externally enhanced $\theta(\eta)$.

Fig. 5 shows impact of suction parameter S on velocity profile $f'(\eta)$, $\boldsymbol{g}(\boldsymbol{\eta})$ and temperature profile $\theta(\eta)$. In this suction parameter S is varying from 2.0 to 2.3 while $\lambda = 1.0, M = 0.2, Ec = 0.2, \varnothing = 0.03, \theta_r = -0.6$ Fig. 5A shows influence of S on velocity profile $f'(\eta)$, when it is varying from 2.0 to 2.3. Fig. 5B shows impact of S on velocity profile $\boldsymbol{g}(\boldsymbol{\eta})$ and 5C shows effect on temperature profile $\theta(\eta)$. 5 A demonstrates that when suction parameter S, increases from 2.0 to 2.3 then velocity profile $f'(\eta)$, decreases. 5B shows that velocity

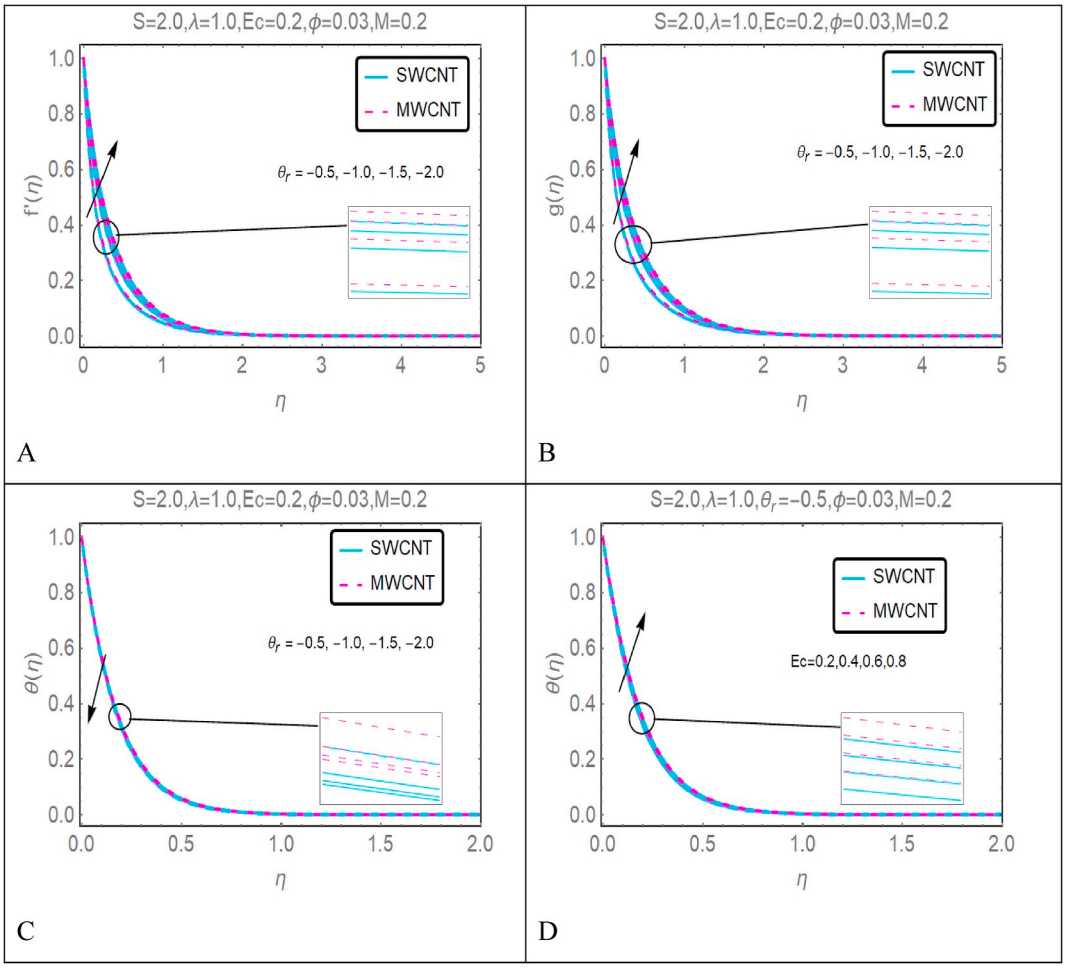

Fig. 6. **(A):** Impact of θ_r on $f'(\eta)$. **(B):** Impact of θ_r on $g(\eta)$. **(C):** Impact of θ_r on $\theta(\eta)$. (D): Impact of Ec on $\theta(\eta)$.

profile $g(\eta)$ also decreasing due to increasing suction parameter. Fig. 5C depicts that temperature profile also decreasing due to increasing suction parameter. A mechanical effect known as suction or injection is utilized to decrease the amount of energy that is lost in the boundary layer region by lowering the amount of drag that is experienced on the surface. This is because elevating the suction parameter leads to a reduction in the boundary layer's velocity as well as its overall thickness. Nanofluids also travel more slowly than ordinary fluids do because of the high viscosity they possess. Therefore, when there is a greater amount of mass suction, the thickness of the thermal boundary layer decreases. When the value of the suction parameter is increased, the temperature drops because a greater quantity of warm fluid is sucked away from the boundary layer. The decline in temperature can be attributed to this factor.

Fig. 6 shows effect of viscosity parameter θ_r on velocity profile $f'(\eta)$, $\boldsymbol{g(\eta)}$ when it varies from $\theta_r = -0.5$ to -2.0 and $\lambda = 1.0, M = 0.2, \varnothing = 0.03, Ec = 0.2, S = 2.0$. It also shows the impact of $\theta_r = -0.5$ to -2.0, Eckert number $Ec = 0.2 - 0.8$ on temperature profile $\theta(\eta)$ when $\lambda = 1.0, M = 0.2, \varnothing = 0.03, Ec = 0.2, S = 2.0$. Fig. 6A demonstrates impact of θ_r on $f'(\eta)$. 6B shows impact of θ_r on $g(\eta)$. 6C shows impact of θ_r on $\theta(\eta)$. Fig. 6D shows the impact of Eckert number E_c, on $\theta(\eta)$. In Fig. 6A when θ_r decreases from -0.5 to -2.0 then velocity profile $f'(\eta)$ increases. Velocity profile $g(\eta)$ increases when θ_r decreases from -0.5 to -2.0 in Fig. 6B. Temperature profile $\theta(\eta)$ decreases when θ_r, decreases in Fig. 6C. In Fig. 6D when Eckert number Ec, increases from 0.2 to 0.8 then temperature profile increases. It ought to go beyond saying that decreasing value of viscosity parameter will result in an increase in size of velocity field. The reason for this is that viscosity is an internal resistive force that works against the flow. Because it is reliant on temperature in this scenario, the viscous forces will decrease as the viscosity drops. It is due to decreasing value of viscous force that increases the fluid velocity. Temperature of fluid decreases with decreasing viscosity parameter because heat energy decreases due to the decrease in flow resistive forces. Large value of Eckert number Ec, is observed to increase temperature profile. Physically, when the Eckert number goes up, it leads to a very strong energy that spreads out, which helps the thermal boundary layer. But when the value of Ec, goes up, heat energy is made, which raises temperature profile of the fluid.

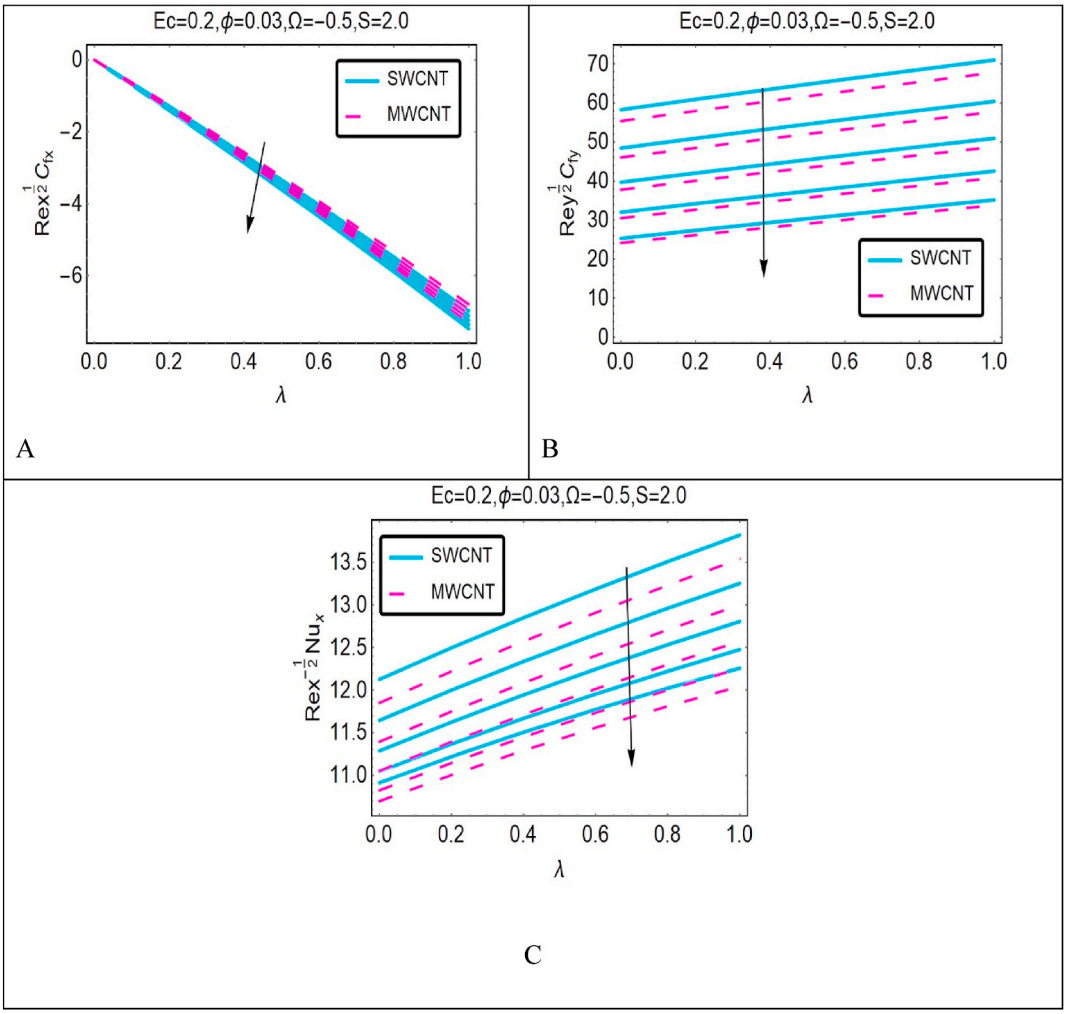

Fig. 7. **(A)** Impact of M and λ on skin friction in $x-$ direction. **(B):** Effect of M and λ on skin friction in $y-$ direction . **(C)**: Impact of M and λ on Nusselt number in $x-$ direction.

4.2. Heat transfer and skin friction

This sub-section provides rate of heat transfer locally, which is written as $\left(\frac{1}{\sqrt{Re_x}} Nu_x\right)$, as well as the skin friction, which is written as $(\sqrt{Re_x} Cf_x$, Both are crucial industrial quantities. The significance of these statistics can't be doubted because of the applications they have in industry. The skin friction coefficients and local Nusselt numbers respond differently to different changes in parameters. The effect of the magnetic parameter M and stretching parameter λ on skin on the skin friction in x, y directions, as well as the Nusselt number in x-direction, is depicted in Fig. 7. Fig. 7A shows impact of magnetic parameter M, stretching parameter λ on skin friction in x direction, 7B in y-direction and 7C shows impact on Nusselt number in x direction. Fig. 7A demonstrates when stretching parameter λ increases from 0 to 1 then skin friction $(\sqrt{Re_x}\, Cf_x)$ decreases in x-direction. Skin friction $(\sqrt{Re_y}\, Cf_y)$ decreases in y-direction when stretching parameter is increased as shown in Fig. 7B. Nusselt number $\left(\frac{1}{\sqrt{Re_x}} Nu_x\right)$, decreases in x-direction when stretching parameter increases from 0 to 1 as shown in Fig. 7C. The Lorentz force, also known as the resistive force, is increased whenever there is a magnetic field present in a fluid that transports electricity. Because of this force, it is more difficult for fluid particles to travel, which results in a reduction in the speed of the fluid (see Fig. 4A). Because of the Lorentz force, the magnetic and electric fields are aligned with one another. Because of this, the fluid that is travelling near the boundary layer moves at a more glacial pace. In a nutshell, as M is increased, the velocity profile is decreased, which results in less frictional drag being exerted on the surface of the sheet. After passing through the stretching sheet, the nanofluid's speed decreases, which causes the momentum boundary layer to become dense. This peculiar trend might have been brought about by the stretching sheet event, which made it more difficult for the nanofluid molecules to pass past the barrier. As the magnetic control becomes more powerful in the nanofluid domain, the thermal boundary layer becomes thicker, as observed in solution, and the rate of heat transmission becomes more gradual. As a result, the rate of heat transfer and

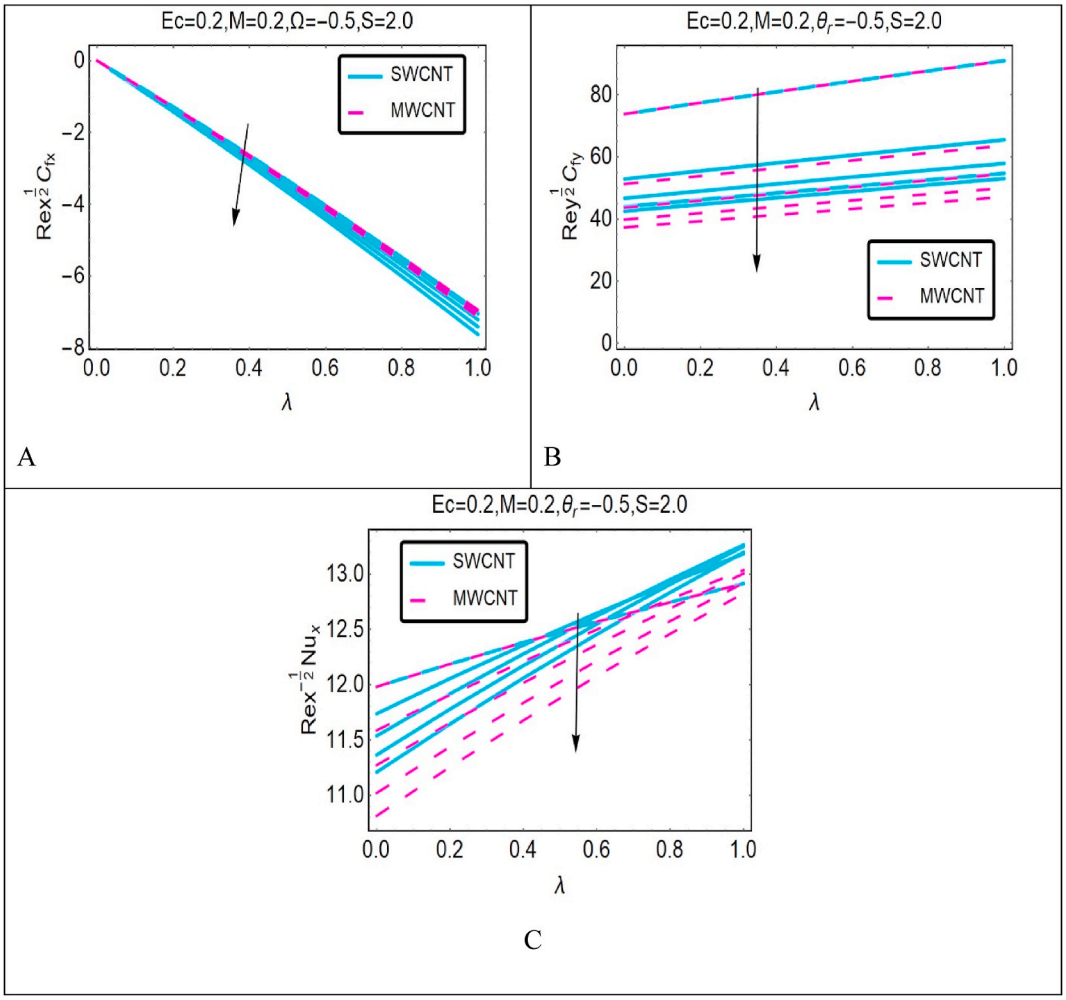

Fig. 8. (A): Impact of φ and λ on skin friction in $x-$ direction. **(B):** Effect of φ and λ on skin friction in $y-$ direction . **(C)**: Impact of φ and λ on Nusselt number in $x-$ direction.

$Re_x^{-1/2} Nu_x$, both decrease because of wall heat flux and stretching of surface.

Fig. 8 shows impact of volume fraction $\varnothing$, stretching parameter λ on skin friction in x and y direction and on Nusselt number in x-direction. Fig. 8A shows impact of volume fraction $\varnothing$, stretching parameter λ on skin friction in x direction, 8B in y-direction and 8C shows impact on Nusselt number in x direction. Fig. 8A demonstrates when stretching parameter λ increases from 0 to 1 due to impact of volume fraction skin friction $(\sqrt{Re_x}\, Cf_x)$ decreases in x-direction. Skin friction $(\sqrt{Re_y}\, Cf_y)$ decreases in y-direction when stretching parameter is increased along with impact of volume fraction as shown in Fig. 8B. Nusselt number $\left(\frac{1}{\sqrt{Re_x}} Nu_x\right)$, decreases in x-direction when stretching parameter increases from 0 to 1 along with impact of volume fraction as shown in Fig. 8C. Fig. 8 illustrates how nanoparticle volume fraction with stretching parameter affect skin friction and Nusselt number. Due to collisions between suspended particles in the flow, drag force will be increased. Thus, the coefficient of friction on the wall will be reduced.

Fig. 9 shows impact of suction limitation S, stretching parameter λ on skin friction in both x and y direction and on Nusselt number in x-direction. Fig. 9A shows impact of suction limitation S, stretching parameter λ on skin friction in x direction, 9B in y-direction and 9C shows impact on Nusselt number in x direction. Fig. 9A demonstrates when stretching parameter λ increases from 0 to 1 along with impact of suction parameter S, skin friction $(\sqrt{Re_x}\, Cf_x)$ decreases in x-direction. Skin friction $(\sqrt{Re_y}\, Cf_y)$ decreases in y-direction when stretching parameter is increased along with impact of S, as shown in Fig. 9B. Nusselt number $\left(\frac{1}{\sqrt{Re_x}} Nu_x\right)$, increases in x-direction when stretching parameter increases from 0 to 1 along with impact of S, as shown in Fig. 9C. It has also been proven that suction parameters stimulus on heat transfer. Fig. 9 reveal impacts of stretching parameter and suction parameter S might vary in many ways. Fig. 9B shows how the value of $\sqrt{Re_y} Cf_y$ increased due to the presence of suction. Nanofluid motion is slowed down, and surface velocity gradient is increased as result of this suction effect at border. When the suction parameter S is present, heat transfer rate increases at surface, as seen in values of $\frac{1}{\sqrt{Re_x}} Nu_x$ shown in Fig. 9C. Heat transfer rate enhanced in proportion to increase in size of suction

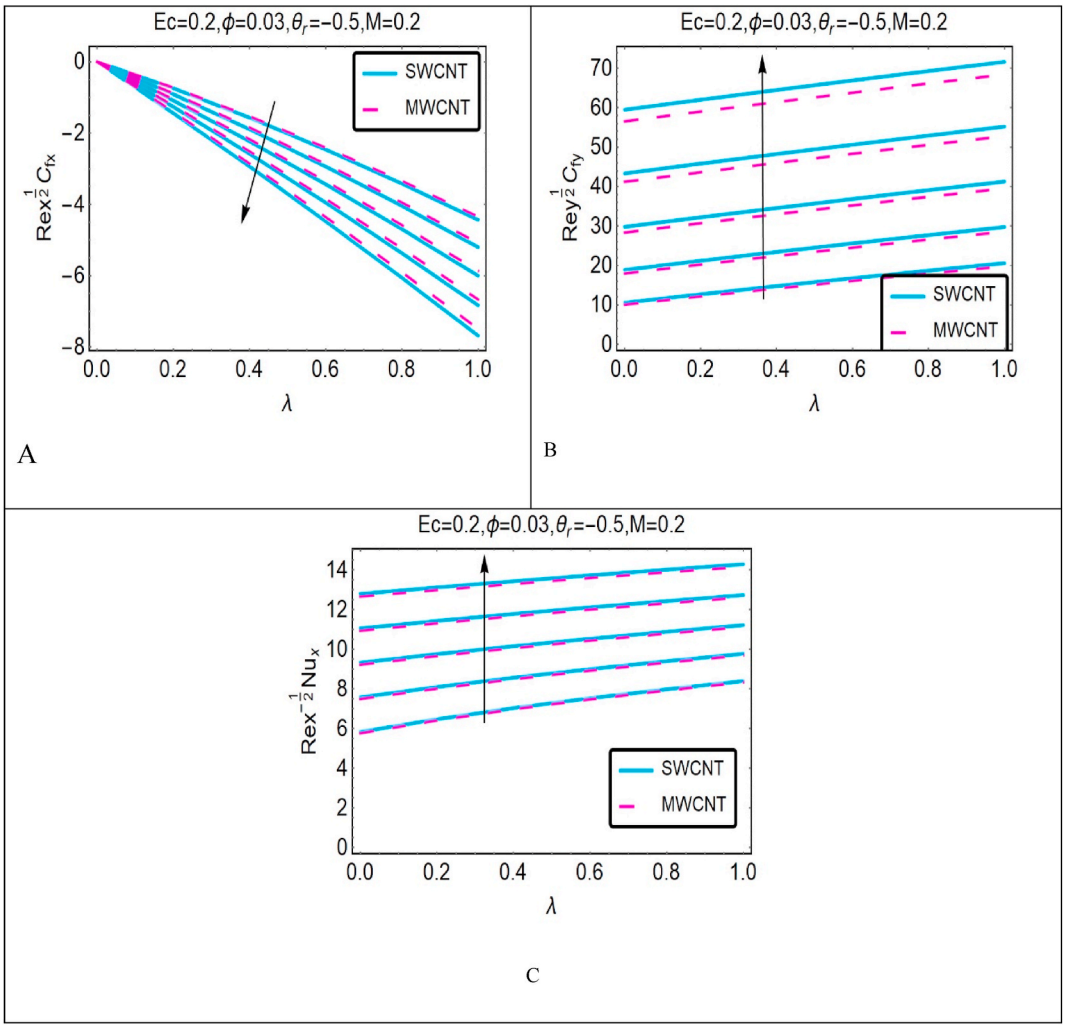

Fig. 9. (A): Impact of S and λ on Skin Friction in $x-$ direction. **(B):** Impact of S and λ on Skin Friction in $y-$ direction . **(C):** Impact of S and λ on Nusselt number in $x-$ direction.

parameter. A rise in value of suction parameter leads to thinner thermal boundary layer that leads to increase in temperature difference between surface and deeper layers of atmosphere.

Fig. 10 shows impact of viscosity parameter θ_r, stretching parameter λ on skin friction in both x, y direction and on Nusselt number in x-direction. It also shows impact of Eckert number E_c with λ on Nusselt number in y-direction. Fig. 10A shows impact of viscosity parameter θ_r, stretching parameter λ on skin friction in x direction, 10B in y-direction and 10C shows impact on Nusselt number in x direction. Fig. 10D shows impact of Eckert number E_c with λ on Nusselt number in x-direction. Fig. 10A demonstrates when λ increases from 0 to 1 along with impact of viscosity parameter θ_r, skin friction $(\sqrt{Re_x}\,Cf_x)$ increases in x-direction. Skin friction $(\sqrt{Re_y}\,Cf_y)$ decreases in y-direction when stretching parameter is increased along with impact of viscosity parameter θ_r, as shown in Fig. 10B. Nusselt number $\left(\frac{1}{\sqrt{Re_x}}Nu_x\right)$, increases in x-direction when stretching parameter increases from 0 to 1 along with impact of viscosity parameter θ_r, as shown in Fig. 10C. Nusselt number $\left(\frac{1}{\sqrt{Re_x}}Nu_x\right)$, also increases in x direction when stretching parameter increases from 0 to 1 along with the impact of Eckert number E_c, as shown in Fig. 10D. Skin friction and Nusselt number increases in x direction it means surface has effect on the fluid and due to impact of Eckert number, Nusselt number decreases as shown in Fig. 10D.

5. Conclusion

This study was done because nanofluid made from carbon nanotubes can be used for many different things in industry. But it also has a lot of physical traits and behaviors that we don't know much about because we have not studied it enough yet. So, this study looks at how the volume fraction, suction, stretching, joule heating, variable viscosity, and MHD affect behavior of reduced skin friction, heat transfer, velocity, and temperature profiles on a three-dimensional carbon nanotubes suspended nanofluid with different length and

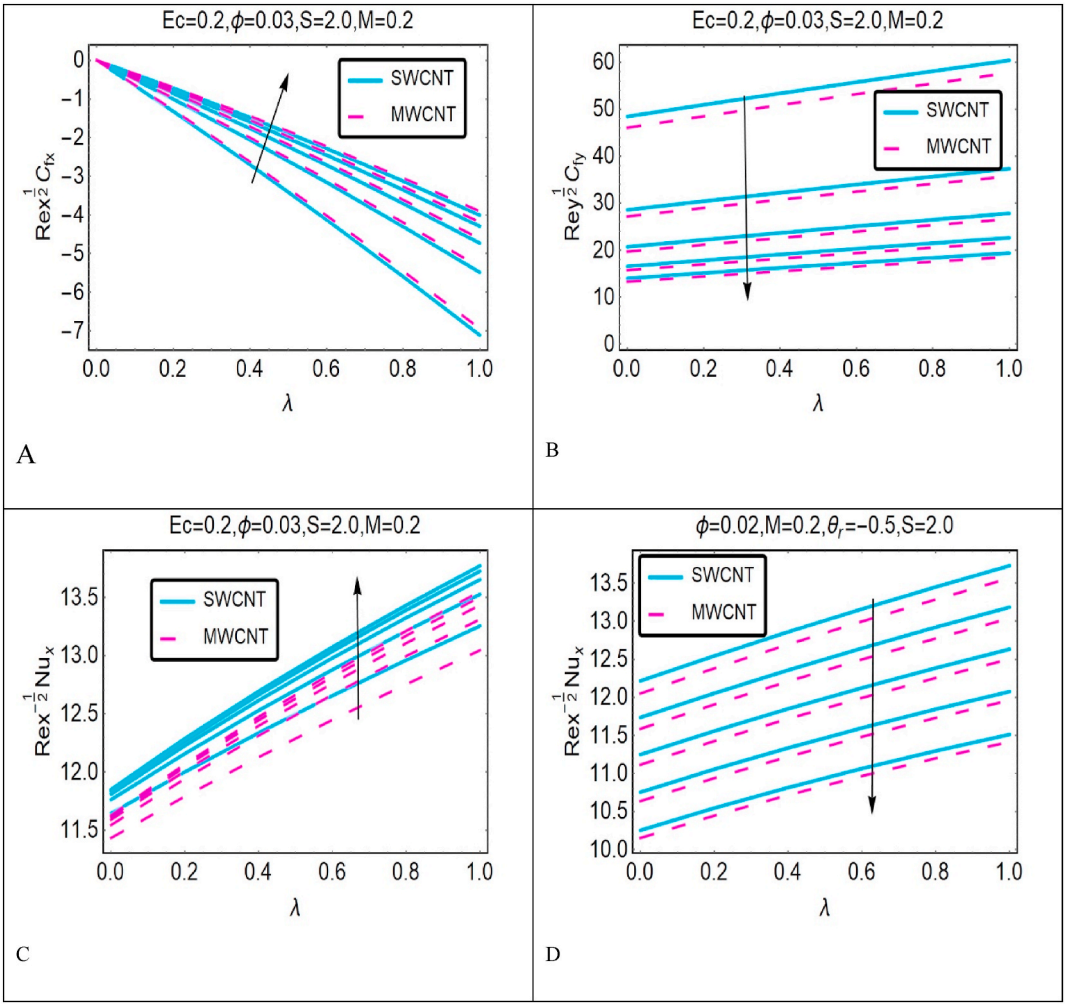

Fig. 10. **(A):** Impact of θ_r and λ on Skin Friction in $x-$ direction. **(B):** Impact of θ_r and λ on Skin friction in $y-$ direction . **(C):** Impact of θ_r and λ on Nusselt number in $x-$ direction. **(D):** Impact of Ec and λ on Nusselt number in $x-$ direction.

radius over a stretching sheet.

Using the RK-IV with shooting method, which runs on the Mathematica computing platform, the above nanofluid flow is solved numerically. To obtain precise numerical and graphical results, a system of higher-order ODEs with corresponding boundary conditions must be solved. These ODEs are transformed from the governing PDEs of the original problem using a technique known as similarity transformation.

The main results of this study can be summed up as follows:

i. Volume fraction of nanoparticles decreases the velocity profiles while enhances the temperature profile.
ii. Suction limitation decreases both velocity and temperature profiles.
iii. When the magnetic parameter goes up, the velocity profile $f^{'}(\eta)$ goes down, but the profile of $\boldsymbol{g}(\boldsymbol{\eta})$ and the temperature both go up at the same time.
iv. When the viscosity parameter goes down, the velocity profile goes up while temperature profile goes down.
v. As the Eckert number goes up, the thermal boundary layer gets thicker.
vi. Skin friction and Nusselt number decreases when stretching parameter increases along with the impacts of magnetic parameter and volume fraction.
vii. An increment in stretching parameter along with impact of suction causes declination in skin friction coefficient in x-direction but at same time, causing increment in skin friction coefficient in y-direction and Nusselt number in x-direction.
viii. An increment in stretching parameter along with impact of viscosity parameter causes an increment in skin friction and Nusselt number in x-direction but at same time causing declination in skin friction in y-direction.
ix. Eckert number causes declination in the Nusselt number in x-direction.

x. The rate of heat transfer increases with the addition of φ and S. When the suction parameter ($S = 2.1$) with 1% of φ is used, it is reported that the rate of heat transfer increases by 1.135% for SWCNTs and 1.275% for MWCNTs.

Author contribution statement

Khadija Rafique: Conceived and designed the experiments; Analyzed and interpreted the data; Contributed reagents, materials, analysis tools or data.

Zafar Mahmood: Conceived and designed the experiments; Contributed reagents, materials, analysis tools or data; Wrote the paper.

Umar Khan: Conceived and designed the experiments; Contributed reagents, materials, analysis tools or data.

Sayed M Eldin: Performed the experiments; Analyzed and interpreted the data.

Alia M. Alzubaidi: Performed the experiments; Wrote the paper.

Data availability statement

Data will be made available on request.

Declaration of competing interest

Authors declare that there is no conflict of interest regarding the publication of this article.

References

[1] S.U.S. Choi, J.A. Eastman, Enhancing Thermal Conductivity of Fluids with Nanoparticles, 1995 International mechanical engineering congress and exhibition, San Francisco, CA (United States), 1995, pp. 12–17. *Nov 1995*, Oct. 01, https://digital.library.unt.edu/ark:/67531/metadc671104/. (Accessed 6 August 2022).

[2] S.U.S. Choi, Z.G. Zhang, W. Yu, F.E. Lockwood, E.A. Gaulke, Anomalous thermal conductivity enhancement in nanotube suspensions, Oct, Appl. Phys. Lett. 79 (14) (2001) 2252–2254, https://doi.org/10.1063/1.1408272.

[3] J. Buongiorno, Convective transport in nanofluids, J. Heat Transf. 128 (3) (Aug. 2005) 240–250, https://doi.org/10.1115/1.2150834.

[4] D.R.L. Hamilton, O.K. Crosser, Thermal conductivity of heterogeneous two-component systems, Ind. Eng. Chem. Fund am., Aug. (1962), https://doi.org/10.1021/i160003a005.

[5] A. Almarashi, et al., Expedition of discharging of energy storage unit with adding nanoparticles using numerical technique, Nov, J. Energy Storage 55 (2022) 105505, https://doi.org/10.1016/j.est.2022.105505.

[6] Z. Li, et al., Amelioration of thermal storage system with inclusion of nanomaterial within solidification, Feb, J. Energy Storage 58 (2023) 106418, https://doi.org/10.1016/j.est.2022.106418.

[7] H.A. Othman, H. Rguigui, S.H. Altoum, Mahjoub A. Elamin, Nanomaterial efficacy on freezing of PCM with involvement of numerical simulation, Sep, J. Mol. Liq. 362 (2022) 119658, https://doi.org/10.1016/j.molliq.2022.119658.

[8] X. Li, et al., Expedition of solidification with dispersing nanoparticles utilizing numerical method, Sep, J. Mol. Liq. 361 (2022) 119640, https://doi.org/10.1016/j.molliq.2022.119640.

[9] L. Qin, H. Ayed, A.M. Alzubaidi, Y.A. Rothan, A.S. Alghawli, H.A. Othman, Examination of treatment of energy storage unit with inclusion of nanomaterial, Sep, J. Energy Storage 53 (2022) 105057, https://doi.org/10.1016/j.est.2022.105057.

[10] H. Ayed, H.A. Othman, Y. Zhang, G.M. Alzabeedy, A.M. Hussin, T.A. Nofal, Thermal storage evaluation in existence of nano-sized additives by mean of numerical method, Nov, J. Energy Storage 55 (2022) 105582, https://doi.org/10.1016/j.est.2022.105582.

[11] V.N. Popov, Carbon nanotubes: properties and application, Mater. Sci. Eng. R Rep. 43 (3) (Jan. 2004) 61–102, https://doi.org/10.1016/j.mser.2003.10.001.

[12] H. Taherian, J.L. Alvarado, E.M. Languri, Enhanced thermophysical properties of multiwalled carbon nanotubes based nanofluids. Part 1: critical review, Feb, Renew. Sustain. Energy Rev. 82 (2018) 4326–4336, https://doi.org/10.1016/j.rser.2017.10.064.

[13] M. Fallah Najafabadi, H. Talebi Rostami, K. Hosseinzadeh, D. domiri ganji, Hydrothermal study of nanofluid flow in channel by RBF method with exponential boundary conditions, Arch. Proc. Inst. Mech. Eng. Part E J. Process Mech. Eng. 1989-1996 Vols (Oct. 2022), https://doi.org/10.1177/09544089221133909.

[14] S. Shakunthala, M.M. Nandeppanavar, Boundary layer flow and cattaneo-christov heat flux of a nonlinear stretching sheet with a suspended CNT, Nanosci. Nanotechnol. - Asia 9 (4) (Dec. 2019) 494–503, https://doi.org/10.2174/2210681208666180821142231.

[15] M.M. Nandeppanavar, S. Shakunthala, Impact of cattaneo-christov heat flux on magnetohydrodynamic flow and heat transfer of carbon nanofluid due to stretching sheet, J. Nanofluids 8 (4) (Apr. 2019) 746–755, https://doi.org/10.1166/jon.2019.1629.

[16] N.S. Akbar, Z.H. Khan, S. Nadeem, The combined effects of slip and convective boundary conditions on stagnation-point flow of CNT suspended nanofluid over a stretching sheet, J. Mol. Liq. 196 (Aug. 2014) 21–25, https://doi.org/10.1016/j.molliq.2014.03.006.

[17] T. Hayat, Z. Abbas, I. Pop, S. Asghar, Effects of radiation and magnetic field on the mixed convection stagnation-point flow over a vertical stretching sheet in a porous medium, Int. J. Heat Mass Tran. 53 (1) (Jan. 2010) 466–474, https://doi.org/10.1016/j.ijheatmasstransfer.2009.09.010.

[18] M.M. Nandeppanavar, N. Raveendra, M.C. Kemparaju, Computational study of consequence of effect of velocity slip on nanofluids with suspended CNTs, Numer. Heat Tran. 0 (0) (Mar. 2023) 1–15, https://doi.org/10.1080/10407782.2023.2178560.

[19] P. Sreedevi, P.S. Reddy, Ali J. Chamkha, Magneto-hydrodynamics heat and mass transfer analysis of single and multi-wall carbon nanotubes over vertical cone with convective boundary condition, Int. J. Mech. Sci. 135 (Jan. 2018) 646–655, https://doi.org/10.1016/j.ijmecsci.2017.12.007.

[20] M.M. Nandeppanavar, S. Shakunthala, Blasius flow and heat transfer of a nanofluid due to flat plate, J. Nanofluids 5 (5) (Oct. 2016) 736–742, https://doi.org/10.1166/jon.2016.1260.

[21] M.M. Nandeppanavar, Melting heat transfer analysis of non-Newtonian Casson fluid due to moving plate, Jan, Eng. Comput. 35 (3) (2018) 1301–1313, https://doi.org/10.1108/EC-04-2017-0148.

[22] M.M. Nandeppanavar, K. MC, N. R, Effect of non-linear thermal radiation on the stagnation point flow of double diffusive free convection due to movingvertical plate, J. Eng. Des. Technol. 21 (1) (Jan. 2021) 150–166, https://doi.org/10.1108/JEDT-10-2020-0430.

[23] A. Mishra, M. Kumar, Velocity and thermal slip effects on MHD nanofluid flow past a stretching cylinder with viscous dissipation and Joule heating, Jul, SN Appl. Sci. 2 (8) (2020) 1350, https://doi.org/10.1007/s42452-020-3156-7.

[24] A. Mishra, M. Kumar, Thermal performance of MHD nanofluid flow over a stretching sheet due to viscous dissipation, joule heating and thermal radiation, Aug, Int. J. Appl. Comput. Math. 6 (4) (2020) 123, https://doi.org/10.1007/s40819-020-00869-4.

[25] A. Mishra, M. Kumar, Influence of viscous dissipation and heat generation/absorption on Ag-water nanofluid flow over a Riga plate with suction, Int. J. Fluid Mech. Res., Jul (2018), https://doi.org/10.1615/InterJFluidMechRes.2018025291.

[26] S. Faghiri, S. Akbari, M.B. Shafii, Kh Hosseinzadeh, Hydrothermal analysis of non-Newtonian fluid flow (blood) through the circular tube under prescribed non-uniform wall heat flux, Theor. Appl. Mech. Lett. 12 (4) (May 2022), 100360, https://doi.org/10.1016/j.taml.2022.100360.

[27] S. Akbari, S. Faghiri, P. Poureslami, K. Hosseinzadeh, M. Behshad Shafii, Analytical solution of non-Fourier heat conduction in a 3-D hollow sphere under time-space varying boundary conditions, Dec, Heliyon 8 (12) (2022), e12496, https://doi.org/10.1016/j.heliyon.2022.e12496.
[28] K. Hosseinzadeh, et al., Investigation of second grade viscoelastic non-Newtonian nanofluid flow on the curve stretching surface in presence of MHD, Dec, Results Eng 17 (2022), 100838, https://doi.org/10.1016/j.rineng.2022.100838.
[29] A. Mishra, M. Kumar, Numerical analysis of MHD nanofluid flow over a wedge, including effects of viscous dissipation and heat generation/absorption, using Buongiorno model, Heat Transf 50 (8) (2021) 8453–8474, https://doi.org/10.1002/htj.22284.
[30] A.C. Eringen, Theory of thermomicrofluids, J. Math. Anal. Appl. 38 (2) (May 1972) 480–496, https://doi.org/10.1016/0022-247X(72)90106-0.
[31] A.M. Salem, Variable viscosity and thermal conductivity effects on MHD flow and heat transfer in viscoelastic fluid over a stretching sheet, Phys. Lett. 369 (4) (Sep. 2007) 315–322, https://doi.org/10.1016/j.physleta.2007.04.104.
[32] M.A. Seddeek, F.A. Salama, The effects of temperature dependent viscosity and thermal conductivity on unsteady MHD convective heat transfer past a semi-infinite vertical porous moving plate with variable suction, Comput. Mater. Sci. 40 (2) (Aug. 2007) 186–192, https://doi.org/10.1016/j.commatsci.2006.11.012.
[33] M.A. Attar, M. Roshani, K. Hosseinzadeh, D. domiri ganji, Analytical solution of fractional differential equations by Akbari–Ganji's method, Sep, Partial Differ. Equ. Appl. Math. 6 (2022) 100450, https://doi.org/10.1016/j.padiff.2022.100450.
[34] K.N. Mehta, S. Sood, Transient free convection flow with temperature dependent viscosity in a fluid saturated porous medium, Aug, Int. J. Eng. Sci. 30 (8) (1992) 1083–1087, https://doi.org/10.1016/0020-7225(92)90032-C.
[35] N. Alipour, B. Jafari, K. Hosseinzadeh, Optimization of wavy trapezoidal porous cavity containing mixture hybrid nanofluid (water/ethylene glycol Go–Al2O3) by response surface method, Jan, Sci. Rep. 13 (2023) 1635, https://doi.org/10.1038/s41598-023-28916-2.
[36] S. Mukhopadhyay, G.C. Layek, Effects of thermal radiation and variable fluid viscosity on free convective flow and heat transfer past a porous stretching surface, Int. J. Heat Mass Tran. 51 (9) (May 2008) 2167–2178, https://doi.org/10.1016/j.ijheatmasstransfer.2007.11.038.
[37] K. Rafique, Z. Mahmood, H. Alqahtani, S.M. Eldin, Various nanoparticle shapes and quadratic velocity impacts on entropy generation and MHD flow over a stretching sheet with joule heating, Alex. Eng. J. 71 (2023) 147–159.
[38] H. TalebiRostami, M. Fallah, K. Hosseinzadeh, and D. D. Ganji, "Investigation of mixture-based dusty hybrid nanofluid flow in porous media affected by magnetic field using RBF method," Int. J. Ambient Energy, pp. 1–32, 637761600000000000, doi: 10.1080/01430750.2021.2023041.
[39] L. Yan, et al., Dual solutions and stability analysis of magnetized hybrid nanofluid with joule heating and multiple slip conditions, Processes 8 (3) (2020), https://doi.org/10.3390/pr8030332. Art. no. 3, Mar.
[40] M.M. Gulzar, A. Aslam, M. Waqas, M.A. Javed, Kh Hosseinzadeh, A nonlinear mathematical analysis for magneto-hyperbolic-tangent liquid featuring simultaneous aspects of magnetic field, heat source and thermal stratification, Dec, Appl. Nanosci. 10 (2020) 4513–4518, https://doi.org/10.1007/s13204-020-01483-y.
[41] W. Cao, S.H. Altoum, H.A. Othman, A.M. Alzubaidi, A.S. Alghawli, Numerical modeling for thermal behavior of nanomaterial laminar flow and convective heat transfer in appearance of magnetic field, Feb, Case Stud. Therm. Eng. 42 (2023) 102727, https://doi.org/10.1016/j.csite.2023.102727.
[42] Yuan Ying Teh, Adnan Ashgar, Three dimensional MHD hybrid nanofluid flow with rotating stretching/shrinking sheet and joule heating, CFD Lett. 13 (8) (Aug. 2021) 1–19, https://doi.org/10.37934/cfdl.13.8.119.
[43] A.H. Ganie, Z. Mahmood, U. Khan, M.Y. Almusawa, Impact of nonlinear thermal radiation on three-dimensional unsteady flow of carbon nanotube-suspended nanofluid with different length and radius of stretching surface, 2023, Int. J. Mod. Phys. C (2023), https://doi.org/10.1142/S0129183124400011.
[44] B. Alqahtani, Z. Mahmood, M.A. Alyami, A.M. Alotaibi, U. Khan, A.M. Galal, Heat and mass transfer analysis of MHD stagnation point flow of carbon nanotubes with convective stretching disk and viscous dissipation, Adv. Mech. Eng. 14 (10) (2022), https://doi.org/10.1177/16878132221128390, p. 16878132221128390, Oct.
[45] K. Vajravelu, K.V. Prasad, C.-O. Ng, The effect of variable viscosity on the flow and heat transfer of a viscous Ag-water and Cu-water nanofluids, Feb, J. Hydrodyn. 25 (1) (2013) 1–9, https://doi.org/10.1016/S1001-6058(13)60332-7.
[46] Nur Syahirah Wahid, et al., Three-dimensional radiative flow of hybrid nanofluid past a shrinking plate with suction, Jul, J. Adv. Res. Fluid Mech. Therm. Sci. 85 (1) (2021) 54–70, https://doi.org/10.37934/arfmts.85.1.5470.
[47] N.S. Khashiie, N.M. Arifin, I. Pop, R. Nazar, E.H. Hafidzuddin, N. Wahi, Three-dimensional hybrid nanofluid flow and heat transfer past a permeable stretching/shrinking sheet with velocity slip and convective condition, Chin. J. Phys. 66 (Aug. 2020) 157–171, https://doi.org/10.1016/j.cjph.2020.03.032.
[48] K. Rafique, Z. Mahmood, S. Saleem, S.M. Eldin, U. Khan, Impact of nanoparticle shape on entropy production of nanofluid over permeable MHD stretching sheet at quadratic velocity and viscous dissipation, Case Stud. Therm. Eng. 4 (5) (2023) 102992.
[49] B.M. Makhdoum, Z. Mahmood, U. Khan, B.M. Fadhl, I. Khan, S.M. Eldin, Impact of suction with nanoparticles aggregation and joule heating on unsteady MHD stagnation point flow of nanofluids over horizontal cylinder, Heliyon 9 (4) (2023).